The increase in cell volume and nuclear number of the koji-fungus *Aspergillus oryzae* contributes to its high enzyme productivity

Ayaka Itani[1], Haruto Motomura[1], Ken Oda[2], Hideyuki Yamashita[3], Kanae Sakai[4], Ken-ichi Kusumoto[4], Shinsuke Shigeto[5], Takehiko Ichikawa[6], Hosain Mohammad Mubarak[6], Takeshi Fukuma[6], Takuya Katayama[7,8], Jun-ichi Maruyama[7,8], Shunsuke Masuo[1], Naoki Takaya[1], Norio Takeshita[1*]

[1] Microbiology Research Center for Sustainability (MiCS), Faculty of Life and Environmental Sciences, University of Tsukuba, Tsukuba, 305-8572, Japan

[2] National Research Institute of Brewing, 3-7-1 Kagamiyama, Higashi-hiroshima, Hiroshima, 739-0046, Japan

[3] Higuchi Matsunosuke Shoten Co., Ltd., 1-14-2 Harima-cho, Abeno-ku, Osaka 545-0022, Japan

[4] Department of Biotechnology, Graduate School of Engineering, Osaka University, 2-1 Yamadaoka, Suita, Osaka 565-0871, Japan

[5] Department of Chemistry, School of Science, Kwansei Gakuin University, Sanda, Hyogo, 669-1330, Japan

[6] Nano Life Science Institute (WPI-NanoLSI), Kanazawa University, Kakuma-machi, Kanazawa 920-1192, Japan

[7] Department of Biotechnology, The University of Tokyo, Tokyo 113-8657, Japan

[8] Collaborative Research Institute for Innovative Microbiology, The University of Tokyo, Tokyo 113-8657, Japan

* Correspondence to: Norio Takeshita, takeshita.norio.gf@u.tsukuba.ac.jp

Abstract

The regulation of cell volume and nuclear number in multi-nucleate organisms remains largely unknown. The koji-fungus *Aspergillus oryzae* has been used in traditional Japanese brewing and fermentation. We discovered that cell volume of hyphae increases tenfold, and the number of nuclei in the hyphal cells also increases tenfold, exceeding 200. The increase in cell volume and nuclear number is unique to *A. oryzae* and correlates with its high enzyme production capabilities. Through transcriptome analysis of thick hyphae isolated via laser microdissection and SNP analysis of practical strains from koji manufacturers, we identified a calcium channel and glycosyl transferase involved in cell volume expansion. Additionally, we indicated that specific amino acids and activation of the TOR pathway are essential for increasing nuclear number. This study not only deepens our understanding of the evolutionary processes that promote high enzyme productivity through fungal breeding, but also provides valuable insights into the molecular mechanisms regulating cell volume and nuclear number in multi-nucleate organisms.

Introduction

In unicellular organisms, cell volume is tightly regulated in coordination with nuclear division timing (1-3). Similarly, in multinucleated filamentous fungi, a correlation exists between cell volume and nuclear number (4, 5). However, the number of nuclei varies across species (6), the factors governing nuclear number and cell volume remain largely unknown. Filamentous fungi are industrially significant microorganisms, and the strains selected through breeding provide ideal research models for studying these evolutionary processes.

Filamentous fungi secrete a variety of hydrolytic enzymes to support their growth, and humans have long harnessed this enzyme secretion ability for the production of a wide range of fermented foods and beverages (7). *Aspergillus oryzae has been used in Japan for over 1,000 years to produce traditional fermented foods like sake, soy sauce, and miso* (8, 9). A distinctive feature of the fermentation techniques is solid-state cultivation using substrates like rice, soybeans, and wheat bran. The inoculum of *A. oryzae* used in fermentation, known as "koji," has been commercially produced for around 700 years (10). Koji is created by cultivating koji-fungus on grains, and koji starter manufacturers have selected and bred strains to improve the flavor and color of various fermented products. The *A. oryzae* strains currently in use are mainly preserved and managed by koji manufacturers and research institutions. A notable characteristic of *A. oryzae* is its high ability to secrete starch-degrading enzymes and proteases, which has led to extensive research into its genome and gene expression regulation (11-17).

Although *A. oryzae* shares 99.5% genomic similarity with *Aspergillus flavus*, which produces the carcinogenic aflatoxin (18), there have been no reports of *A. oryzae* producing aflatoxins, and its safety has been confirmed at the molecular level (19, 20). Phylogenomic analyses suggest that *A. oryzae* and *A. flavus* diverged approximately 50,000 to 189,000 years ago (21, 22). Over the following millennia, human use of *A. oryzae* is thought to have driven significant genomic

64 recombination, resulting in its evolution into a "cell factory" specifically optimized for the breakdown
65 of sugars and proteins (23).

66 Additionally, modern biotechnology utilizes filamentous fungi as cell factories to produce
67 organic acids, enzymes, and pharmaceuticals (24-26). *A. oryzae* also shows high production capacity
68 as a host for both homologous and heterologous protein production in modern biotechnology (27, 28).
69 Recently, its application has expanded to include the production of pharmaceutical proteins and
70 secondary metabolites (29, 30). Furthermore, filamentous fungi involved in fermentation play a crucial
71 role in creating a more sustainable food system, such as by upcycling agricultural by-products into
72 food through fungal fermentation and using A. oryzae mycelium for alternative meats (31, 32).

73 While basic and applied research on *A. oryzae* continues, fundamental questions remain
74 unanswered, such as why *A. oryzae* exhibits high enzyme production capacity and why it excels as a
75 host for heterologous expression. This study shows that the key lies in the increase in cell volume and
76 nuclear number, and analyzes the molecular mechanisms.

77

78 **Result**

79 **Increase in nuclear number and cell volume in *Aspergillus oryzae***

80 In the model strain *A. oryzae* RIB40, hyphae on day 1 of cultivation contain 10-20 nuclei per cell, but
81 by day 2 of cultivation, apical cells with more than 200 nuclei appear (33). We found that the
82 proportion of hyphae with a higher number of nuclei (represented by class III, over 200 nuclei in the
83 cell, see methods) increased as the culture period increased from 1 to 3 days (Fig. 1A, B) (33). This
84 phenotype was not observed in the model fungus *Aspergillus nidulans* or the closely related species *A.*
85 *flavus* (Fig. 1A, B) (33). As far as we know, such phenotypes have not been observed in other strains
86 of *Aspergillus nidulans*, *Aspergillus niger*, *Aspergillus fumigatus*, or other strains commonly used in
87 research. Among other *Aspergillus* species used in fermentation (9, 10), the proportion of hyphae with

88 a higher number of nuclei increased in *Aspergillus sojae*, which is used for miso and soy sauce
89 production. This phenotype was not observed in *Aspergillus luchuensis* nor in its albino mutant
90 *Aspergillus luchuensis mut. kawachii*, which are used for distilled spirits such as awamori and shochu.
91 Among several strains of *A. oryzae* used in industrial applications, the RIB915 strain used for soy
92 sauce fermentation does not show an increase in the number of nuclei, while the RIB128 and RIB430
93 strains used in sake brewing exhibit a significant increase in the number of nuclei, suggesting that
94 different phenotypes were selected through distinct breeding processes.

95 The distribution of nuclei in the hyphae of *A. oryzae* RIB40 was visualized through 3D
96 reconstruction (Fig. 1C, Movie 1). In the class I hyphae, the nuclei were spaced relatively evenly,
97 whereas in the class III hyphae with increased nuclei, the nuclei were densely packed and arranged in
98 a disordered manner. Furthermore, the nuclear size in the class III hyphae was significantly smaller
99 than that in the class I hyphae (Fig. 1D, E).

100 Strains without an increase in nuclear number had hyphae with diameters ranging from 2 to
101 7 μm, while strains with an increase in nuclear number had some hyphae of similar thickness but often
102 exhibited thicker hyphae exceeding 10 μm (Fig. 1F). The number of nuclei and cell volume in hyphae
103 at 100 μm from the tips were compared among *A. oryzae* strains (RIB40, RIB128, RIB915) and *A.*
104 *flavus* (Fig. 1G). A strong positive correlation was observed between number of nuclei and cell volume.
105 This is consistent with previously reports that the number of nuclei per hyphal volume remains
106 constant (4, 5).

107

108 **Thick hyphae with increased nuclei emerge by branching**

109 Time-lapse imaging using the *A. oryzae* RIB40 expressing H2B-GFP indicated that thick hyphae with
110 increased nuclei emerged by branching from hyphae without increased nuclei (Fig. 2A, Movie 2). In
111 the emerged thick hyphae, rapid nuclear division occurred at the sites of branching (Fig. 2B, Movie

3). Immediately after branching, the thick hyphae showed a significantly faster rate of nuclear proliferation, increasing 4–5 times within 8 hours compared to the thin hyphae immediately after branching (Fig. 2C). Branches from hyphae with increased nuclei produced both hyphae with and without increased nuclei (Fig. 2D).

Time-lapse imaging was conducted over a wider area, and image processing was applied to color-code the nuclei: green for those in hyphae with increased nuclei and white for those in hyphae without increased nuclei (Fig. 2E, Movie 4, Fig.S1A, see methods). Up to 24 hours after inoculation, most hyphae were thin with no increase in nuclei number, but thick hyphae with increased nuclei began to appear as time progressed (Fig. 2E, F). Since thick hyphae elongated faster than thin hyphae (Fig. 2G), thick hyphae outgrew and overtook thin hyphae, eventually dominating the colony perimeter (Fig. 2E, F).

Transmission electron microscopy confirmed basic nuclear structures, such as the nuclear membrane and nucleolus, in both thick and thin hyphae (Fig. S1B). As hyphal diameter increased, cell walls became more uneven and thicker (Fig. 2H, I). This finding corresponds with Raman spectroscopy results showing pronounced peaks corresponding to cell wall polysaccharides in thick hyphae (Fig. S1C)(34). Additionally, peaks associated with active mitochondria were prominent in thick hyphae (Fig. S1C)(35), which was further confirmed by fluorescence staining (Fig. S1D). The surface structure and mechanical properties of the cell wall were analyzed using atomic force microscopy. Thick hyphae exhibited greater surface roughness and higher elasticity compared to thin hyphae (Fig. 2J, K, Fig. S1E, F).

Correlation between nuclear number and enzyme secretion

We compared the amounts of secreted proteins in *A. oryzae* RIB40, RIB128, RIB915, *A. nidulans*, and *A. flavus* (Fig. 3A). The strains that show an increase in nuclear number had significantly higher levels

136 of protein secretion than the strains that do not. In this condition, α-amylases are the dominant proteins
137 secreted by *A. oryzae* (15). The amylase enzyme activity was compared between in *A. oryzae* RIB40,
138 which shows an increase in nuclear number, and *A. oryzae* RIB915, which does not show an increase.
139 In RIB40, starting from day 2, when hyphae with increased nuclear numbers appeared, the enzyme
140 activity per fungal biomass significantly increased more than RIB915 (Fig. 3B).

141 To compare the amylase activity between hyphae with a higher and a lower number of nuclei,
142 amylase activity was monitored under conditions where a single hypha grew in a microfluidic channel
143 with a fluorescent substrate (Fig. 3C, S2A, Movie 5)(36). After 12 hours, the fluorescence intensity in
144 the channel with thick hyphae was about three times higher than that in the channel with thin hyphae,
145 indicating that thicker hyphae secreted more amylase than thinner hyphae (Fig. 3D).

146 We found that addition of yeast extract increased in both hyphal width and nuclear number
147 in the RIB915 strain (Fig. 3E, Fig. S2B), whereas adding yeast extract to *A. nidulans* did not result in
148 an increase in hyphal width or nuclear number. In *A. oryzae* RIB40, the addition of yeast extract did
149 not make the already thick hyphae any thicker but increased the proportion of thicker hyphae. Addition
150 of yeast extract increased protein secretion approximately 1.8 times in RIB40 and 8.5 times in RIB915
151 (Fig. 3F).

152 The addition of nucleic acids, peptone, or casamino acids to the minimal medium increased
153 the number of nuclei in *A. oryzae* RIB915, while vitamin B did not cause a significant change in
154 nuclear number (Fig. S2C). Although the addition of individual amino acids did not show the same
155 effect as yeast extract, the addition of asparagine, proline, glutamine, and branched-chain amino acids
156 increased the proportion of hyphae with increased nuclei by 40-50% (Fig. 3G, Fig. S2D). The amino
157 acids that induced nuclear number increase also led to an increase in protein secretion, indicating a
158 positive correlation between the ratio of class III hyphae and the increase in secreted proteins (Fig. 3H,
159 Fig. S2E). Since the amino acids inducing an increase in nuclear number may activate the TOR

160 pathway (37), *A. oryzae* RIB40 was grown with low concentration of rapamycin, a TOR pathway
161 inhibitor, which minimally affects colony size. Under the conditions, RIB40 did not produce hyphae
162 with an increased number of nuclei (Fig. 3I-K, Fig. S2F).
163
164 **Transcriptome analyses in hyphae with increased nuclei**
165 To investigate gene expression changes in hyphae with increased nuclei, transcriptome analysis was
166 performed under six conditions: In minimal medium; *A. oryzae* RIB40, which shows increased nuclei,
167 *A. oryzae* RIB915 and *A. nidulans*, which do not show increased nuclei. In minimal medium with yeast
168 extract, *A. oryzae* RIB40 and RIB915, which shows increased nuclei, and *A. nidulans,* which do not
169 show increased nuclei (Fig. 4A, Fig. S2B). In RIB915, supplementation with yeast extract led to a
170 more than four-fold increase in the expression of 660 genes, among which 449 genes did not show
171 such increase in RIB40 or *A. nidulans* (Fig. 4B, Table S1). GO analysis of these genes revealed that
172 processes related to cell wall synthesis and divalent metal ion transport were significantly enriched
173 (Fig. 4C).
174 To capture gene expression changes associated with increased nuclei with higher resolution,
175 thick and thin hyphae from RIB40 were dissected using laser microdissection, collected separately,
176 and subjected to transcriptome analysis (Fig. 4D, Movie 6). Clear differences in gene expression
177 pattern were observed between thick and thin hyphae (Fig. 4E). 558 genes that were more than four-
178 fold upregulated in thick hyphae but not in thin hyphae (Table S2). GO analysis of the upregulated
179 genes indicated an enrichment of processes related to biogenesis of ribosome and cellular component
180 (Fig. 4F). Among them, 21 matched those from Table S1 (Fig. 4G, Table S3). Of these, 13 had GO
181 annotations, which were related to conidiation, cell wall synthesis, Ca^{2+} transport and rRNA
182 processing (Fig. 3H). KEGG map visualization indicates that overall ribosomal gene expression
183 increased in the thick hyphae than the thin hyphae (Fig. S3A).

184 Among the gene list, we focused on *msy1* and *msy2*, which are involved in Ca^{2+} transport
185 and maintaining cell volume homeostasis in *Schizosaccharomyces pombe* (38, 39). Disruption of the
186 orthologue genes, *msyA* and *msyB,* in *A. oryzae* RIB40 did not have a significant impact on colony
187 growth, hyphal morphology and number of nuclei in minimal medium (Fig. S3B). Under hypoosmotic
188 shock conditions, the Δ*msyA* often indicated cell lysis near the hyphal tips (Fig. 4I, J). Under
189 hypoosmotic conditions, water influx into the cells causes hyphal cell expansion, but the volume and
190 turgor pressure are regulated to prevent cell lysis. The *msyA* disruption, however, impairs the
191 regulation of the hyphal cell expansion, leading to hyphal lysis (Fig. S3C-E).
192
193 **SNP analysis among industrial strains with distinct phenotypes**
194 The fact that currently used *A. oryzae* strains are managed and preserved by koji manufacturers and
195 research institutions is a notable advantage of *A. oryzae* research. Whole-genome sequencing and
196 comparative genome analysis of 82 *A. oryzae* strains with different applications have shown that these
197 strains cluster into several clades (24). We investigated whether nuclear numbers increase in 20 strains
198 selected from six different clades (Fig. 5A). In the minimal media supplemented with yeast extract, all
199 strains exhibited an increase in nuclear number (Fig. S4A). In the minimal media without yeast extract,
200 three strains from Clade C showed an increase in nuclear number, whereas strains from Clades A, B,
201 and E did not (Fig. 5A, B, Fig. S4A). Clades F and G included both strains with increased nuclear
202 numbers and strains without. SNP analysis of ORFs in Clades F and G revealed 108 mutations in
203 Clade F between TK-32 and TK-38, and 23 mutations in Clade G between TK-41 and TK-47 (Table
204 S4 and S5).
205 Among these, AO090038000626; *rseA*, predicted glycosyl transferase, was the only
206 common gene. This gene has been identified as a mutation in a *A. sojae* mutant with high extracellular
207 enzyme production (40). It is also shown that deletion of *rseA* in *A. nidulans* leads to cell wall defects

208 and promotes enzyme secretion (40). Comparison of mutations in *rseA* among strains in Clade C, F
209 and G indicates a few amino acid substitutions within the ORF, but no common mutations
210 corresponded to the phenotype (Fig. 5C, Fig. S4B). Structural prediction suggests that the mutations
211 are located inside the enzyme domain (Fig. S4C).

212 The disruption of the *rseA* in *A. oryzae* RIB40 resulted in significant growth delay, increased
213 branching, and the absence of hyphae with increased nuclei (Fig. 5D, Fig. S4D). The *rseA* gene DNA
214 fragments from the strains with increased nuclei (RIB40, TK-47) or from the strain without increased
215 nuclei (TK-41) were amplified by PCR and introduced ectopically into RIB915 (Fig. 5E). The strains
216 expressing *rseA* from RIB40 or TK-47 exhibited an increase in hyphal width and a corresponding
217 increase in the proportion of hyphae with more nuclei, whereas the strain expressing *rseA* from TK41
218 showed no increase in hyphal width or nuclear number (Fig. 5E, F, Fig. S4E).

219

220 **Industrial breeding strains from other genera**

221 To investigate whether the phenomenon of increased nuclear numbers also applies to other industrial
222 fungi, we compared the bred strain of *Trichoderma reesei* (QM9414) for cellulase production and its
223 control strain (QM6a)(41), as well as the bred strain of *Penicillium chrysogenum* (IFO4688) for
224 penicillin production and wild type strain (42). In minimal medium, no significant differences in
225 hyphal width or nuclear number were observed between the bred and control strains, whereas with the
226 addition of yeast extract, a notable increase in nuclear number and hyphal width was observed only in
227 the bred strains (Fig. 5G, H, Fig. S5A-C). The addition of yeast extract significantly increased cellulase
228 and protease activity only in the bred strain of *T. reesei* and *P. chrysogenum,* respectively (Fig. 5I, J).
229 These results suggest that even in modern biotechnology, where high enzyme or compound producing
230 strains are bred, strains with increased nuclear numbers were selected, like the traditional breeding
231 practices of koji-fungi.

232

233 **Discussion**

234 In *A. oryzae* some strains, hyphae grow about three times thicker and contain roughly ten times more
235 nuclei than the initial hyphae (Fig. 1). These thicker hyphae emerge from existing branches, where
236 nuclear division is promoted, resulting in the formation of hyphae with an increased number of nuclei
237 (Fig. 2). A clear correlation was observed between hyphal cell volume and nuclear number (Fig. 1G).
238 This consistency aligns with findings in other organisms, from unicellular yeast to multicellular plants
239 and animals, where the nuclear-to-cytoplasmic ratio is tightly regulated, allowing cell cycle
240 progression only upon reaching a critical cell size (1-3). Both the G1/S and G2/M transitions are
241 controled by size checkpoints, with specific mechanisms differing between species (44, 45).

242 In *A. nidulans*, it is known that the duration of the G1 and G2 phases is regulated by
243 temperature (46). While the mechanisms governing the G1/S phase transition remain unclear (47), the
244 G2/M phase transition has been shown to involve the following: During the interphase of *A. nidulans*,
245 NimX (CDK1) binds to NimE (cyclin B), and its activity is regulated through phosphorylation by
246 AnkA (Wee1 kinase) and NimT (Cdc25 phosphatase)(48-50). The activated NimX-NimE complex
247 subsequently dephosphorylates by NimT and activates NimA (Never-in-Mitosis A) protein kinase (51,
248 52). NimA is essential for the transition from G2 to mitosis, and its expression is tightly regulated
249 during the cell cycle (52). The mRNA level of *nimA* and *nimT* begin to increase in G2, reach a plateau
250 during late G2 and M phases, and are sharply degraded at the end of mitosis upon re-entry into
251 interphase (52, 53), meaning high expression levels of *nimA* and *nimT* result in a longer G2 phase. In
252 thick hyphae, *nimA* and *nimT* mRNA was hardly detected, suggesting that thick hyphae sense cell
253 volume in some way and subsequently shorten the G2 phase (Fig. S6A).

254 Branching emerges as a result of cell wall loosening at the branching site. SNP analysis
255 between industrial strains with different phenotypes identified RseA, a predicted glycosyltransferase

256 (Fig. 5). Deletion of *rseA* caused defects in cell wall synthesis in *A. nidulans*, leading to increased
257 enzyme secretion (40, 54). Although the targets of RseA are unknown, RseA could be involved in the
258 cell wall integrity by modifying glycosyl chains on enzymes responsible for cell wall synthesis and
259 degradation. Mutations in *rseA* may impair the regulation of cell wall loosening at the branching site,
260 resulting in the formation of thicker hyphae. In fact, in the thick hyphae of RIB40, localized
261 imbalances in cell wall components have been demonstrated by TEM and AFM.

262 Thicker hyphae can only form if high turgor pressure is maintained within the hyphae, in
263 addition to changes in cell wall remodeling during branching. *msyA* and *msyB*, whose orthologues are
264 calcium channels involved in the regulation of cell volume, were identified among the genes that show
265 a significant increase in expression in thicker hyphae (Fig. 4)(38, 39). Analysis of the knockout strains
266 demonstrated the function of cell volume regulation adapted to increased turgor pressure in
267 hypoosmotic conditions. The function of these calcium channels is likely crucial for maintaining the
268 balance of turgor pressure and cell volume.

269 The Target of Rapamycin (TOR) pathway is a central regulator of cellular growth,
270 responding to a variety of nutrients, such as amino acids, and carbon sources, as well as environmental
271 factors like oxygen levels, osmotic pressure, pH, and temperature stress (55, 56). Upon sensing these
272 inputs, the TOR pathway influences translation activity, metabolic flow, and cell size (56, 57). In both
273 yeast and mammalian models, amino acids like branched-chain amino acids (BCAAs), glutamine, and
274 alanine are crucial for nutrient sensing, forming the basis for TOR signaling activation (57-59). These
275 amino acids are like those contributing to nuclear increase in the RIB915 strain (Fig. 3G). Furthermore,
276 TOR inhibition by rapamycin in the RIB40 strain suppressed the formation of hyphae with increased
277 nuclei (Fig. 3I-K). Consistent with the activation of translation by the TOR pathway, the expression
278 of ribosome-related genes was elevated in thicker hyphae (Fig. S3A). The TOR pathway directly
279 regulates mitochondrial activity (60). Thick hyphae exhibited heightened mitochondrial density and

280 activity (Fig. S1C, D), suggesting that the TOR pathway support the high ATP demand associated with
281 rapid biosynthesis.

282 Cell volume and nuclear number mutually regulate each other, meaning that thicker hyphae
283 always possess more nuclei. For the formation of thicker hyphae with numerous nuclei, an increase in
284 cell volume and a corresponding increase in nuclei must occur simultaneously (Fig. S6A). In our
285 model, mutations in *rseA* loosen the cell wall during branching, and the regulation of turgor pressure
286 and cell volume by MsyA represents the necessary condition to increase cell volume and maintain
287 thick hyphae. At the same time, enhanced translational capacity involving TOR activation and
288 mechanisms that accelerate the cell cycle constitute another essential condition enabling an increase
289 in nuclear number.

290 *A. nidulans* and *A. flavus* did not exhibit an increase in nuclear number. *A. sojae* displayed
291 increased nuclear numbers, whereas *A. kawachii* and *A. luchuensis* did not (Fig. 1). The 20 strains of
292 *A. oryzae* selected from different clades showed an increase in nuclear number in the minimal medium
293 supplemented with yeast extract. In the medium without yeast extract, there were strains that showed
294 an increase in nuclear number and others that did not. These differences might be due to variations in
295 their applications or the selection of strains with diverse characteristics, such as not only enzyme
296 activity but also their impact on the flavor, aroma, and color of the final products. Additionally, there
297 might be dominant mutations that activate TOR pathway even in the minimal medium. Multiple gene
298 mutations were identified as contributing to the phenotype of increased hyphal volume and nuclear
299 number, suggesting that the phenotype was not the result of a single mutation but rather the gradual
300 accumulation of mutations through breeding. The koji-fungus strains used to produce high-quality
301 sake and soy sauce have been selectively bred over many years, long before the advent of modern
302 biotechnology, to enhance their saccharolytic and proteolytic activities. Modern biotechnological bred
303 strains such as *T. reesei* QM9414 and *P. chrysogenum* IFO4688 also exhibit a phenotype of thicker

hyphae with increased nuclear numbers under nutrient-rich conditions (Fig. 5). This consistency suggests that by breeding naturally multinucleate filamentous fungi under nutrient-rich conditions, it is possible to obtain strains with increased nuclear numbers and enhanced enzyme or compound production.

The number of nuclei in filamentous fungi varies greatly among species (61). For example, *Neurospora crassa* can exceed 100 nuclei, which correlates with its exceptionally rapid growth rate and high protein secretion capacity (62). An increase in the number of nuclei per cell is expected to enhance transcription and translation per cell, thereby improving enzyme production and secretion capacity (Fig. S6B). However, maintaining a high nuclear number requires a substantial amount of energy, and in conditions where external nutrient supply is insufficient, cells rapidly die. Thus, the tendency to maintain a high nuclear number could be a selective pressure unlikely to occur in nature. Koji-kin strains were bred specifically for high enzyme production in nutrient-rich environments, and we propose that some of them acquired the specialized trait of increased cell volume and nuclear number through selection. This study elucidates the evolutionary processes driven by breeding selection in *A. oryzae* and the underlying mechanisms contributing to high enzyme productivity. These findings not only offer new approaches for optimizing filamentous fungi for bioindustry applications but also lead to the elucidation of the molecular mechanisms regulating cell volume and nuclear number in multinucleated organisms.

Acknowledgements.

This work was funded by MEXT KAKENHI grant number 21H02095, 21K19062 and Scientific Research on Innovative Areas “Post-Koch Ecology” grant number 22H04878 to NT. Ohsumi Frontier Science Foundation, Noda Institute for Scientific Research Grant, and Japan Science and Technology Agency (JST) ERATO grant number JPMJER1502 to NT. AFM measurement was supported by the World Premier International Research Center Initiative (WPI).

Methods

Strains and Culture Conditions. The filamentous fungal strains used in this study are listed in Table S6. *A. oryzae* RIB40 expressing H2B-GFP, UtH2BG stain, is described previously (33). Minimal medium for *Aspergillus* species was shown in Table S7. When peptone, casamino acids, or yeast extract was added, the final concentration was 1%. Amino acids were added at a final concentration of 0.1%, B vitamins (biotin, pyridoxine hydrochloride, thiamin hydrochloride, riboflavin, PABA, and nicotinic acid) were added at 100 μM, and nucleotides (inosine and uridine) were added at 10 mM.

Genetic Manipulation. To delete target genes, genome editing plasmids and circular donor DNA plasmids were constructed as described previously (63). The sgRNA cassette was designed under the U6 promoter with the following target sequences: GTGACGATCTACGGTAACGC for the *msyA* gene, GATCAGTTGAGCGTCCCCTA for the *msyB* gene, and AGCTAGCGCAGCCGGTCTGC for the *rseA* gene. The genome editing plasmid was constructed by introducing the sgRNA expression cassette into the *Sma*I restriction site of the pRGE-gRT6 plasmid (63). For the donor plasmid, 1 kb fragments upstream and downstream of the target genes were amplified, ligated, and inserted into the linearized pUC19 vector (Takara Bio). Both plasmids were applied for transformation using the *A. oryzae* RIB40 strain. To amplify the *RseA* region, spanning 1 kb upstream to 1 kb downstream, the templates used were *A. oryzae* RIB40, TK-42, and TK-47 strains. The amplified fragments were inserted into the *Hind*III site of the pPTRI vector (TaKaRa) to construct the plasmid. Transformations were performed using the protoplast-PEG method according to the manufacturer's protocol for pPTRI. Transformants were selected on the minimal medium plates containing 0.1 mg/l pyrithiamine. Integration of constructs was confirmed by PCR analysis.

Microscopy. Images were captured using an Axio Observer Z1 inverted epifluorescence microscope (Carl Zeiss) equipped with Plan-Apochromat objectives, an AxioCam 506 mono camera, and a Colibri.2 LED light source. The stage temperature was maintained at 30°C with thermoplate (Tokai Hit). Nuclei were stained with SYBR Green (Takara), mitochondrial ware stained with Rhodamine 123 (Invitrogen), cell membrane were stained with FM4-64 (Invitrogen). Images were collected using Zen (Carl Zeiss) and ImageJ software.

Image Analysis. The distribution pattern of nuclei was classified into the following three types; Class I: nuclei distribute at a constant interval without overlapping; Class II: nuclei align but sometimes overlap; Class III: nuclei scattered throughout hyphae but not aligned. Nuclei, hyphal size, and fluorescence intensity were quantified using Zen and ImageJ software. Z-stack 3D reconstruction and nuclear color coding were performed with Imaris (Oxford Instruments). Hyphal elongation distances were analyzed using the MTrackJ plugin in ImageJ. For Fig. 2E, nuclei were binarized, and those in non-increased hyphae were displayed in white based on size and circularity.

Transmission Electron Microscopy (TEM). The culture samples were embedded in 1% water agar

367 and fixed with 2.5% glutaraldehyde in 0.1 M phosphate buffer (pH 7.0) at room temperature for 2
368 hours. Sample preparation and sectioning were performed at the Institute of Medicine, University of
369 Tsukuba. Observations were conducted using a JEM-1400 transmission electron microscope (JEOL).
370 **Imaging with Microfluidic Devices.** Microfluidic devices were fabricated as described previously
371 (33). Two types of devices were constructed: a 2D observation device to visualize hyphal expansion
372 (Fig. S1A) and a single-hypha isolation device for enzymatic activity measurement (Fig. S2A).
373 Conidia suspensions were loaded into a 10 ml plastic syringe (SS-10ESZ, Terumo) and connected to
374 polyethylene tubing (inner diameter 0.38 mm, outer diameter 1.09 mm, BD Intramedic). Air was
375 expelled from the syringe, and the suspension was injected into the device inlet. The number of conidia
376 flowing through the microfluidic channel was adjusted under a microscope. The syringe was then
377 replaced with another containing medium, and the medium was delivered at the minimum flow rate
378 using a syringe pump (YSP-101, YMC). The device was incubated at 30°C on a thermal stage (TOKAI
379 HIT) and imaged using an Axio Observer Z1 microscope (Carl Zeiss). α-amylase activity in the device
380 was measured using the EnzChek Ultra amylase assay kit (Invitrogen).
381 **Enzyme Activity Assays.** Fungal conidia 10^4 were inoculated onto 25 ml of medium in a petri dish
382 and statically cultured at 30 ºC for 4 days. Protein concentration and enzymatic activities in the culture
383 supernatant were measured. Protein quantification was performed using the Bradford assay (Protein
384 Assay Kit, BIO-RAD), with bovine gamma globulin as the standard. Carboxymethyl cellulase
385 (CMCase) activity was determined by measuring reducing sugars using the 3,5-dinitrosalicylic acid
386 method. CMCase activity was assayed at 50 ºC for 15 min in a reaction mixture containing 50 mM
387 sodium acetate buffer (pH 5.0) and 1% carboxymethyl cellulose. One unit of enzyme activity was
388 defined as the amount of enzyme required to release 1 μmol of reducing sugar (as glucose equivalent)
389 per minute. α-amylase activity was measured using an α-Amylase Assay Kit (Kikkoman Biochemifa)
390 according to the manufacturer's instructions. Acid carboxypeptidase (ACP) activity was determined
391 using the Acid Carboxypeptidase Assay Kit (Kikkoman Biochemifa) following the provided protocol.
392 **RNA-seq Analysis.** Sterilized cellophane was placed on agar plates, and conidia were inoculated.
393 After culturing at 30 ºC for 3 days, samples were frozen, homogenized with a mortar and pestle, and
394 total RNA was extracted using the RNeasy Mini Kit (QIAGEN). Library preparation, sequencing, and
395 partial data analysis were performed by the Faculty of Medicine, University of Tsukuba. Sequencing
396 was conducted using 36 bp paired end reads on the Illumina NextSeq 500, and reads were mapped to
397 the *A. oryzae* RIB40 reference genome using the CLC Genomic Workbench (QIAGEN). For laser
398 microdissection, sterilized membrane slides (Carl Zeiss) were immersed in MM liquid, and conidia
399 were inoculated onto the membrane. After static culturing at 30 ºC for 3 days, sections were collected
400 using a PALM MicroBeam laser microdissection system (Carl Zeiss). RNA was extracted from 500-
401 700 sections respectively using the RNeasy Mini Kit. Library preparation and sequencing were
402 performed by Takara Bio Inc., using 150 bp paired end reads on the Illumina NovaSeq 6000. Reads

were mapped to the *A. oryzae* RIB40 reference genome using the CLC Genomic Workbench. Genes showing a ≥4-fold change in expression were considered significant, and gene ontology (GO) enrichment analysis of biological processes was performed using ShinyGO 0.81 (64). Heatmaps were visualized using the Python Seaborn package (65). Gene annotations were obtained from FungiDB.

Low Osmotic Pressure Shock Analysis. Conidia were spot inoculated onto the minimal medium containing 1 M NaCl and cultured at 30 ºC for 3 days. Colony tips were treated with distilled water for 3 min, and the number of tip ruptures was counted. Hyphal tip swelling was assessed by staining hyphae cultured in the minimal medium liquid for 3 days with FM4-64, mounting them on a coverslip with a small volume of medium, and adding an equal volume of distilled water.

Raman Spectroscopy. The conidia were inoculated into minimal medium liquid in a glass-bottom dish and cultured at 30 ºC for 3 days. Raman spectra were acquired using an XploRA PLUS Raman microscope, as described previously (32). Hyphae attached to the dish bottom were irradiated with a 532 nm laser at 0.93 mW for 30 seconds. Spike artifacts caused by cosmic rays were manually removed. Ten spectra were averaged, and background signals attributed to the medium and glass were subtracted.

Protein Structure Analysis. RseA protein structure was predicted using AlphaFold2 and visualized with PyMOL (v1.20). Domains were annotated using InterPro.

Atomic Force Microscopy (AFM). The conidia were inoculated into minimal medium liquid on a Poly-L-Lysine-coated (Sigma Aldrich) glass-bottom dish (ibidi) and cultured at 30 ºC for 3 days. We used a JPK Nanowizard 4 (Bruker) equipped with an inverted fluorescence microscope (Eclipse Ti2, Nikon). The temperature was maintained at 30 ºC using a dish heater integrated into the stage. BL-AC40TS-C2 cantilevers (Olympus, spring constant approximately 0.1 N/m) were used for AFM imaging under the following conditions: QI mode, 1.5 × 1.5 μm or 0.5 × 0.5 μm scan size, 128 × 128 pixels, Z-length 1 μm, setpoint 0.1 nN, and Z speed 166 μm/s. The Young's modulus was calculated using JPKSPM Data Processing software (Bruker). After averaging and baseline subtraction, Young's modulus was calculated using a Hertz model with a triangular pyramid half-cone angle of 35°.

SNP analysis. The genome data of *A. oryzae* required for SNP identification was obtained from the National Center for Biotechnology Information (NCBI). and mapped to *A. oryzae* RIB40 reference sequence using BWA-MEM2 (64). The SNPs were listed by FreeBayes (67), and detailed comparative analysis of genomes was performed on Integrative Genome Viewer (IGV) manually.

RNA seq. The RNA seq data have been deposited in DDBJ as BioProject PRJDB19992.

434

435 References

436 1. Amodeo, A. A. & Skotheim, J. M. Cell-Size Control. *Cold Spring Harb Perspect Biol* **8**,
437 a019083 (2016).
438 2. Nurse, P. Genetic control of cell size at cell division in yeast. *Nature* **256**, 547–551 (1975).
439 3. Jorgensen, P. *et al.* The Size of the Nucleus Increases as Yeast Cells Grow. *MBoC* **18**, 3523–
440 3532 (2007).
441 4. Dynesen J, Nielsen J. Branching is coordinated with mitosis in growing hyphae of *Aspergillus*
442 *nidulans*. *Fungal Genet Biol* 40, 15-24 (2003).
443 5. Dundon SE, Chang SS, Kumar A, Occhipinti P, Shroff H, Roper M, Gladfelter AS. Clustered
444 nuclei maintain autonomy and nucleocytoplasmic ratio control in a syncytium. *Mol Biol Cell*
445 **27**, 2000-7(2016).
446 6. Roper, M., Ellison, C., Taylor J. W. & Glass N. L. Nuclear and Genome Dynamics in
447 Multinucleate Ascomycete Fungi. *Curr Biol* **21**, R786-793 (2011).
448 7. Hurst, C. J. Microbial Fermentations in Nature and as Designed Processes. John Wiley & Sons
449 Ltd. (2023)
450 8. Kitamoto, K. Cell biology of the *Koji* mold *Aspergillus oryzae*. *Biosci, Biotechnol, Biochem* **79**,
451 863–869 (2015).
452 9. Ichishima, E. Development of enzyme technology for *Aspergillus oryzae*, *A. sojae*, and *A.*
453 *luchuensis,* the national microorganisms of Japan. *Bioscience, Biotechnology, and*
454 *Biochemistry* **80**, 1681–1692 (2016).
455 10. Yamashita, H. Koji Starter and Koji World in Japan. *JoF* **7**, 569 (2021).
456 11. Machida, M. *et al.* Genome sequencing and analysis of *Aspergillus oryzae*. *Nature* **438**, 1157–
457 1161 (2005).
458 12. Machida, M., Yamada, O. & Gomi, K. Genomics of Aspergillus oryzae: Learning from the
459 History of Koji Mold and Exploration of Its Future. *DNA Research* **15**, 173–183 (2008).
460 13. Gomi, K. Regulatory mechanisms for amylolytic gene expression in the koji mold *Aspergillus*
461 *oryzae*. *Bioscience, Biotechnology, and Biochemistry* **83**, 1385–1401 (2019).
462 14. Tanaka, M. & Gomi, K. Induction and Repression of Hydrolase Genes in *Aspergillus*
463 *oryzae*. *Front. Microbiol.* **12**, 677603 (2021).
464 15. Wang, B. *et al.* Survey of the transcriptome of *Aspergillus oryzae* via massively parallel mRNA
465 sequencing. *Nucleic Acids Research* **38**, 5075–5087 (2010).
466 16. Ishida, H. *et al.* Identification of functional elements that regulate the glucoamylase-encoding
467 gene (*glaB*) expressed in solid-state culture of *Aspergillus oryzae*. *Current Genetics* **37**, 373–
468 379 (2000).
469 17. Kitano, H., Kataoka, K., Furukawa, K. & Hara, S. Specific expression and temperature-

470 dependent expression of the acid protease-encoding gene (*pepA*) in *Aspergillus oryzae* in solid-
471 state culture (Rice-Koji). *J Biosci Bioengineering* **93**, 563–567 (2002).
472 18. Rokas, A. *et al.* What can comparative genomics tell us about species concepts in the genus
473 *Aspergillus*? *Studies in Mycology* **59**, 11–17 (2007).
474 19. Kusumoto, K.-I., Nogata, Y. & Ohta, H. Directed deletions in the aflatoxin biosynthesis gene
475 homolog cluster of *Aspergillus oryzae*. *Current Genetics* **37**, 104–111 (2000).
476 20. Kobayashi, T. *et al.* Genomics of *Aspergillus oryzae*. *Biosci, Biotechnol, Biochem* **71**, 646–670
477 (2007).
478 21. Watarai, N., Yamamoto, N., Sawada, K. & Yamada, T. Evolution of *Aspergillus oryzae* before
479 and after domestication inferred by large-scale comparative genomic analysis. *DNA Res* **26**,
480 465–472 (2019).
481 22. Chang, P.-K. & Ehrlich, K. C. What does genetic diversity of *Aspergillus flavus* tell us about
482 *Aspergillus oryzae*? *Internat J Food Microbiol* **138**, 189–199 (2010).
483 23. Gibbons, J. G. *et al.* The Evolutionary Imprint of Domestication on Genome Variation and
484 Function of the Filamentous Fungus *Aspergillus oryzae*. *Current Biol* **22**, 1403–1409 (2012).
485 24. Meyer, V. *et al.* Current challenges of research on filamentous fungi in relation to human
486 welfare and a sustainable bio-economy: a white paper. *Fungal Biol Biotechnol* **3**, 6, s40694-
487 016-0024–8 (2016).
488 25. Liu, D., Garrigues, S. & de Vries, R. P. Heterologous protein production in filamentous
489 fungi. *Appl Microbiol Biotechnol* **107**, 5019–5033 (2023).
490 26. Meyer, V. *et al.* Growing a circular economy with fungal biotechnology: a white paper. *Fungal*
491 *Biol Biotechnol* **7**, 5 (2020).
492 27. Christensen, T. *et al.* High Level Expression of Recombinant Genes in *Aspergillus oryzae. Nat*
493 *Biotechnol* **6**, 1419–1422 (1988).
494 28. Saito, N., Katayama, T., Minami, A., Oikawa, H. & Maruyama, J. Versatile filamentous fungal
495 host highly-producing heterologous natural products developed by genome editing-mediated
496 engineering of multiple metabolic pathways. *Commun Biol* **7**, 1263 (2024).
497 29. Huynh, H. H. *et al.* Functional production of human antibody by the filamentous fungus
498 *Aspergillus oryzae*. *Fungal Biol Biotechnol* **7**, 7 (2020).
499 30. Itoh, T., Tokunaga, K., Matsuda, Y. *et al.* Reconstitution of a fungal meroterpenoid biosynthesis
500 reveals the involvement of a novel family of terpene cyclases. *Nature Chem* **2**, 858–864 (2010).
501 31. Maini Rekdal, V., Villalobos-Escobedo, J.M., Rodriguez-Valeron, N. *et al. Neurospora*
502 *intermedia* from a traditional fermented food enables waste-to-food conversion. *Nat*
503 *Microbiol* **9**, 2666–2683 (2024).
504 32. Maini Rekdal, V., van der Luijt, C.R.B., Chen, Y. *et al.* Edible mycelium bioengineered for
505 enhanced nutritional value and sensory appeal using a modular synthetic biology toolkit. *Nat*

Commun **15**, 2099 (2024).

33. Yasui M, Oda K, Masuo S, Hosoda S, Katayama T, Maruyama JI, Takaya N, Takeshita N. Invasive growth of *Aspergillus oryzae* in rice koji and increase of nuclear number. *Fungal Biol Biotechnol*. 7, 8 (2020).
34. Hossain IM, Mazumder N, Kaino T, Kawamukai M, Noothalapati H, Yamamoto T. Direct Visualization of Structurally Similar Polysaccharides in Single Yeast Cells in Vivo by Multivariate Analysis Assisted Raman Microspectroscopy. *J Phys Chem B* 127, 5249-5256 (2023).
35. Yasuda, M., Takeshita, N. & Shigeto, S. Inhomogeneous Molecular Distributions and Cytochrome Types and Redox States in Fungal Cells Revealed by Raman Hyperspectral Imaging Using Multivariate Curve Resolution–Alternating Least Squares. *Anal. Chem.* **91**, 12501–12508 (2019).
36. Itani, A., Shida, Y. & Ogasawara, W. A microfluidic device for simultaneous detection of enzyme secretion and elongation of a single hypha. *Front. Microbiol.* **14**, 1125760 (2023).
37. Wouters, B. G. & Koritzinsky, M. Hypoxia signalling through mTOR and the unfolded protein response in cancer. *Nat Rev Cancer* **8**, 851–864 (2008).
38. Nakayama, Y., Yoshimura, K. & Iida, H. Organellar mechanosensitive channels in fission yeast regulate the hypo-osmotic shock response. *Nat Commun* **3**, 1020 (2012).
39. Nakayama, Y., Hirata, A. & Iida, H. Mechanosensitive channels Msy1 and Msy2 are required for maintaining organelle integrity upon hypoosmotic shock in *Schizosaccharomyces pombe*. *FEMS Yeast Res* **14**, 992–994 (2014).
40. Ogawa, M. *et al.* Deletion of *Aspergillus nidulans cpsA/rseA* induces increased extracellular hydrolase production in solid-state culture partly through the high osmolarity glycerol pathway. *J Biosci Bioeng* **131**, 589–598 (2021).
41. Vitikainen, M. *et al.* Array comparative genomic hybridization analysis of Trichoderma reesei strains with enhanced cellulase production properties. *BMC Genomics* **11**, 441 (2010).
42. Barreiro, C., Martín, J. F. & García-Estrada, C. Proteomics Shows New Faces for the Old Penicillin Producer *Penicillium chrysogenum*. *J Biomed Biotechnol* **2012**, 1–15 (2012).
43. Murphy, C. M. & Michael, W. M. Control of DNA Replication by the Nucleus/Cytoplasm Ratio in Xenopus. *J Biol Chem* **288**, 29382–29393 (2013).
44. Futcher, B. & Kellogg, D. R. SnapShot: Cell size control. *Cell* **187**, 2896-2896.e1 (2024).
45. Fantes, P. & Nurse, P. Control of cell size at division in fission yeast by a growth-modulated size control over nuclear division. *Experiment Cell Research* **107**, 377–386 (1977).
46. Bergen, L. G. & Morris, N. R. Kinetics of the nuclear division cycle of *Aspergillus nidulans*. *J Bacteriol* **156**, 155–160 (1983).
47. Dörter, I. & Momany, M. Fungal Cell Cycle: A Unicellular versus Multicellular

542 Comparison. *Microbiol Spectr* **4**, 4.6.28 (2016).
543 48. Gould, K. L. & Nurse, P. Tyrosine phosphorylation of the fission yeast cdc2+ protein kinase
544 regulates entry into mitosis. *Nature* **342**, 39–45 (1989).
545 49. Wu, L., Osmani, S. A. & Mirabito, P. M. A Role for NIMA in the Nuclear Localization of
546 Cyclin B in *Aspergillus nidulans*. *J Cell Biol* **141**, 1575–1587 (1998).
547 50. Ye, X. S., Fincher, R. R., Tang, A. & Osmani, S. A. The G2/M DNA damage checkpoint
548 inhibits mitosis through Tyr15 phosphorylation of p34cdc2 in *Aspergillus nidulans*. *EMBO*
549 *J* **16**, 182–192 (1997).
550 51. Shen, K. F. & Osmani, S. A. Regulation of mitosis by the NIMA kinase involves TINA and its
551 newly discovered partner, An-WDR8, at spindle pole bodies. *MBoC* **24**, 3842–3856 (2013).
552 52. Osmani, S. A., May, G. S. & Morris, N. R. Regulation of the mRNA levels of *nimA*, a gene
553 required for the G2-M transition in *Aspergillus nidulans*. *J Cell Biol* **104**, 1495–1504 (1987).
554 53. Osmani, A. H., O'Donnell, K., Pu, R. T. & Osmani, S. A. Activation of the *nimA* protein kinase
555 plays a unique role during mitosis that cannot be bypassed by absence of the *bimE* checkpoint.
556 *EMBO J* **10**, 2669–2679 (1991).
557 54. Feng, X. *et al. cpsA* regulates mycotoxin production, morphogenesis and cell wall biosynthesis
558 in the fungus *Aspergillus nidulans*. *Mol Microbiol* **105**, 1–24 (2017).
559 55. Urban, J. *et al.* Sch9 Is a Major Target of TORC1 in *Saccharomyces cerevisiae*. *Molecular*
560 *Cell* **26**, 663–674 (2007).
561 56. De Virgilio, C. & Loewith, R. The TOR signalling network from yeast to man. *The Internat J*
562 *Biochem Cell Biol* **38**, 1476–1481 (2006).
563 57. Kim, J. & Guan, K.-L. mTOR as a central hub of nutrient signalling and cell growth. *Nat Cell*
564 *Biol* **21**, 63–71 (2019).
565 58. Saxton, R. A. & Sabatini, D. M. mTOR Signaling in Growth, Metabolism, and
566 Disease. *Cell* **169**, 361–371 (2017).
567 59. Meng, D. *et al.* Glutamine and asparagine activate mTORC1 independently of Rag GTPases. *J*
568 *Biol Chem* **295**, 2890–2899 (2020).
569 60. Düvel, K. *et al.* Activation of a Metabolic Gene Regulatory Network Downstream of mTOR
570 Complex 1. *Mol Cell* **39**, 171–183 (2010).
571 61. Roper, M., Ellison, C., Taylor J. W. & Glass N. L. Nuclear and Genome Dynamics in
572 Multinucleate Ascomycete Fungi. *Curr Biol* **21**, R786-793 (2011).
573 62. Havlik, D., Brandt, U., Bohle, K. & Fleißner, A. Establishment of *Neurospora crassa* as a host
574 for heterologous protein production using a human antibody fragment as a model product.
575 *Microbial Cell Factories* **16**, 128 (2017).
576 63. Katayama, T. *et al.* Forced Recycling of an AMA1-Based Genome-Editing Plasmid Allows for
577 Efficient Multiple Gene Deletion/Integration in the Industrial Filamentous Fungus *Aspergillus*

oryzae. *Appl Environ Microbiol* **85**, e01896-18 (2019).

64. Ge, S. X., Jung, D. & Yao, R. ShinyGO: a graphical gene-set enrichment tool for animals and plants. *Bioinformatics* **36**, 2628–2629 (2020).
65. Waskom, M. seaborn: statistical data visualization. *JOSS* **6**, 3021 (2021).
66. Vasimuddin, M., Misra, S., Li, H. & Aluru, S. Efficient Architecture-Aware Acceleration of BWA-MEM for Multicore Systems. *IEEE Parallel and Distributed Processing Symposium (IPDPS)*, 314-324 (2019)
67. Garrison, E. & Marth, G. Haplotype-based variant detection from short-read sequencing. arXiv:1207.3907 [q-bio.GN] https://doi.org/10.48550/arXiv.1207.3907

591 **Figure legends.**

592 Figure 1. Increase in number of nuclei and cell volume in *Aspergillus* species. (A) The nuclear
593 distribution in the tip cells was categorized into Classes I–III. The ratio of hyphae in each class was
594 measured in *Aspergillus* species at 24, 48, and 72 hours of growth (n=50). Data for *A. oryzae* RIB40
595 and *A. nidulans* are reproduced from a previous study (33). (B) Colony morphology after 3 days of
596 culture on the minimal medium. The nuclear distribution in the hyphae at the colony periphery stained
597 with SYBR Green. Scale bars: hyphae, 20 μm; colonies, 1 cm. (C) 3D images of hyphae without
598 increased nuclei (left) and with increased nuclei (right) in *A. oryzae* RIB40 from Movie 1. Each
599 nucleus is indicated with different colors by Imaris soft. Scale bar: 5 μm. (D) Comparison of nuclear
600 size in Class I hyphae (2.4 μm) and Class III hyphae (1.6 μm), indicated by white lines. (E) Box plots
601 of nucleus diameters in hyphae without increased nuclei and those with increased nuclei (n=35, ** p
602 < 0.01, t-test). (F) Box plots of hyphal width at the colony periphery grown for 72 hours (n=10–14, **
603 $p< 0.01$, * $p< 0.05$, t-test). Strains with increased nuclei are marked in red, and those without are
604 marked in blue. (G) Correlation between nuclear number and cell volume of hyphae at 100 μm from
605 the tips in *A. oryzae* RIB40, RIB128, RIB915, and *A. flavus*.

606

607 Figure 2. Thick hyphae with increased nuclei emerge by branching. (A) Time-lapse image sequence
608 of *A. oryzae* RIB40 expressing H2B-GFP showing the emergence of thick hyphae with increased
609 nuclei by branching from Movie 2. Scale bar: 20 μm. Elapsed time is indicated in min. (B) Image
610 sequence of successive nuclear division within the newly emerged branched hypha from Movie 3.
611 Scale bar: 10 μm. Elapsed time is indicated in min. (C) Time course of nuclear number per hypha.
612 Nuclear numbers were counted with the start time of branching set as 0, every hour for 5 to 10 h.
613 Thick; hyphal width >7 μm, Thin; hyphal width <5 μm. (D) Branching from hyphae with increased
614 nuclei generates both thick hyphae with increased nuclei (left) and thin hyphae without increased

615 nuclei (right). Scale bars: 20 μm. (E) Image sequence of mycelial growth showing hyphae with
616 increased nuclei (green) and without increased nuclei (white) from Movie 4. Scale bars: 200 μm.
617 Elapsed time is indicated in h. (F) Line histogram of hyphal width at the colony periphery at 20, 40,
618 and 60 h, calculated from Movie 4 (n=40). (G) Correlation between hyphal width and maximum
619 elongation rate calculated from Movie 4 (n=45). The maximum elongation rate is determined from
620 elongation rates measured every hour over 10 hours period. (H) TEM images of *A. oryzae* RIB40
621 hyphae. Hyphal diameter and cell wall thickness are indicated white and black text respectively. Scale
622 bar: 1 μm. (I) Correlation plots of hyphal width and cell wall thickness based on TEM images. Thick
623 hyphae (>7 μm) are marked in red, and thin hyphae (<7 μm) are marked in blue. (J) 3D surface images
624 of *A. oryzae* RIB40 hyphal tips in the thick hypha (upper) and the thin hypha (lower) constructed using
625 AFM. (K) Surface roughness of cell walls in thick (red) and thin (blue) hyphae along the arrows in J.
626
627 Figure 3. Correlation between number of nuclei and enzyme secretion. (A) Secreted protein per
628 biomass in strains with increased nuclei (red) and without increased nuclei (blue) after 4 days of culture
629 in minimal medium with 1% maltose (mean ± S.E., n=3, ** $p < 0.01$, t-test). (B) Time course of α-
630 amylase activity per biomass in *A. oryzae* RIB40 and RIB915 cultured in minimal medium with 1%
631 maltose (mean ± S.E., n=3). (C) Measurement of α-amylase activity in a single hypha using a
632 microfluidic device. A fluorescent substrate increases in fluorescence upon hydrolysis by α-amylase.
633 ROIs for thick hypha are marked in red, and thin hypha in blue. Scale bar: 10 μm. (D) Temporal
634 changes in fluorescence intensity measured in individual flow channels, as described in C. (E) Box
635 plots of hyphal width in colonies grown in minimal medium with or without 1% yeast extract (n=10–
636 18, ** $p < 0.01$, * $p < 0.05$, t-test). Conditions with increased nuclei are marked in red, and those
637 without in blue. (F) Secreted protein per biomass in minimal medium with or without 1% yeast extract
638 (mean ± S.E., n=3, ** $p < 0.01$, t-test). (G) Ratio of class I-III hyphae in *A. oryzae* RIB915 colonies

639 grown in minimal medium supplemented with 1% yeast extract or 0.1% individual amino acids (n=50).
640 (H) Correlation between the ratio of Class III hyphae and secreted protein per biomass in the 0.1%
641 amino acid-supplemented medium. (I) Images of hyphae and nuclear distribution in *A. oryzae* RIB40
642 grown on minimal medium with or without 0.5 ng/ml rapamycin. Scale bars: 10 μm. (J) Ratio of class
643 I-III hyphae in *A. oryzae* RIB40 cultured on minimal medium containing 0, 0.5, 5, or 100 ng/ml
644 rapamycin (n=50). (K) Box plots of hyphal width in the colonies cultured under the conditions in J
645 (n=11-18, ** $p < 0.01$, t-test).
646
647 Figure 4. Transcriptome analyses in hyphae with increased nuclei. (A) Heatmap of gene expression in
648 *A. oryzae* RIB40, RIB915, and *A. nidulans* grown in the minimal medium with or without 1% yeast
649 extract. The top 500 genes with the largest variation in expression are shown. (B) Venn diagram of
650 genes upregulated more than four-fold in the medium with yeast extract. (C) GO process analysis of
651 genes uniquely upregulated in *A. oryzae* RIB915 grown in the medium with yeast extract. (D) Image
652 sequence of cutting and collecting the targeted hypha by using laser microdissection. Scale bar: 100
653 μm. (E) Heatmap of gene expression in thick (n=3) and thin (n=2) hyphae dissected from *A. oryzae*
654 RIB40. The top 300 genes with the largest expression differences are shown. (F) GO process analysis
655 of genes upregulated more than four-fold in thick hyphae compared to thin hyphae. (G) Venn diagram
656 of 449 genes upregulated in RIB915 with yeast extract and 558 genes upregulated in thick hyphae of
657 RIB40. (H) GO annotations of 13 genes from the 21 shared genes in G. Genes related to cell wall
658 processes are shown in green, cell membrane in blue, Ca^{2+} transport in yellow, and rRNA processing
659 in orange. (I) Images of hyphae of RIB40 and Δ*msyA* strains after 3 min of low osmotic stress. Scale
660 bar: 200 μm. (J) Ratio of hyphal tip lysis under the hypoosmotic shock (mean ± S.E., n=50, ** $p <$
661 0.01, t-test).
662

Figure 5. Comparison of industrial bred strains in *A. oryzae, T. reesei* and *P. chrysogenum*. (A) Phylogenetic clade A-F of *A. oryzae* TK strains. The strains with increased nuclei are indicated in red. (B) Colonies and hyphae stained with SYBR Green of strains in clades C, F, and G grown for 3 days on the minimal medium. Scale bar: 20 µm. (C) Sequence differences in *rseA* gene among strains in clades C, F, and G. UTR regions are marked in pink, exons in purple, and nucleotide differences in white. (D) Colonies and hyphae stained with SYBR Green of RIB40 and the Δ*rseA* strain grown for 3 days on the minimal medium. Scale bar: 10 µm. (E) Colonies and hyphae stained with SYBR Green of RIB915 expressing *rseA* gene from RIB40 and TK-47 strains with increased nuclei, and TK-41 strain without increased nuclei. Scale bar: 20 µm. (F) Hyphal width of RIB915 and strains in E (n=14–23). Strains with *rseA* from strains with increased nuclei are marked in red, and those without are marked in blue. (G) Hyphal images stained with SYBR Green of *T. reesei* (QM9414) and *P. chrysogenum* (IFO4688) grown for 3 days on the minimal medium with or without 1% yeast extract. Scale bar: 20 µm. (H) Ratio of class I-III hyphae in the *T. reesei* and *P. chrysogenum* control and bred strains cultured on the minimal medium with or without 1% yeast extract for 3 days (n=50). (I) CMCase activity per biomass of *T. reesei* industrial and control strains under the conditions in G (mean ± S.E., n=3, ** $p < 0.01$, t-test). (J) Protease activity per biomass of *P. chrysogenum* industrial and control strains under the conditions in G (mean ± S.E., n=3, ** $p < 0.01$, t-test).

Fig. 1

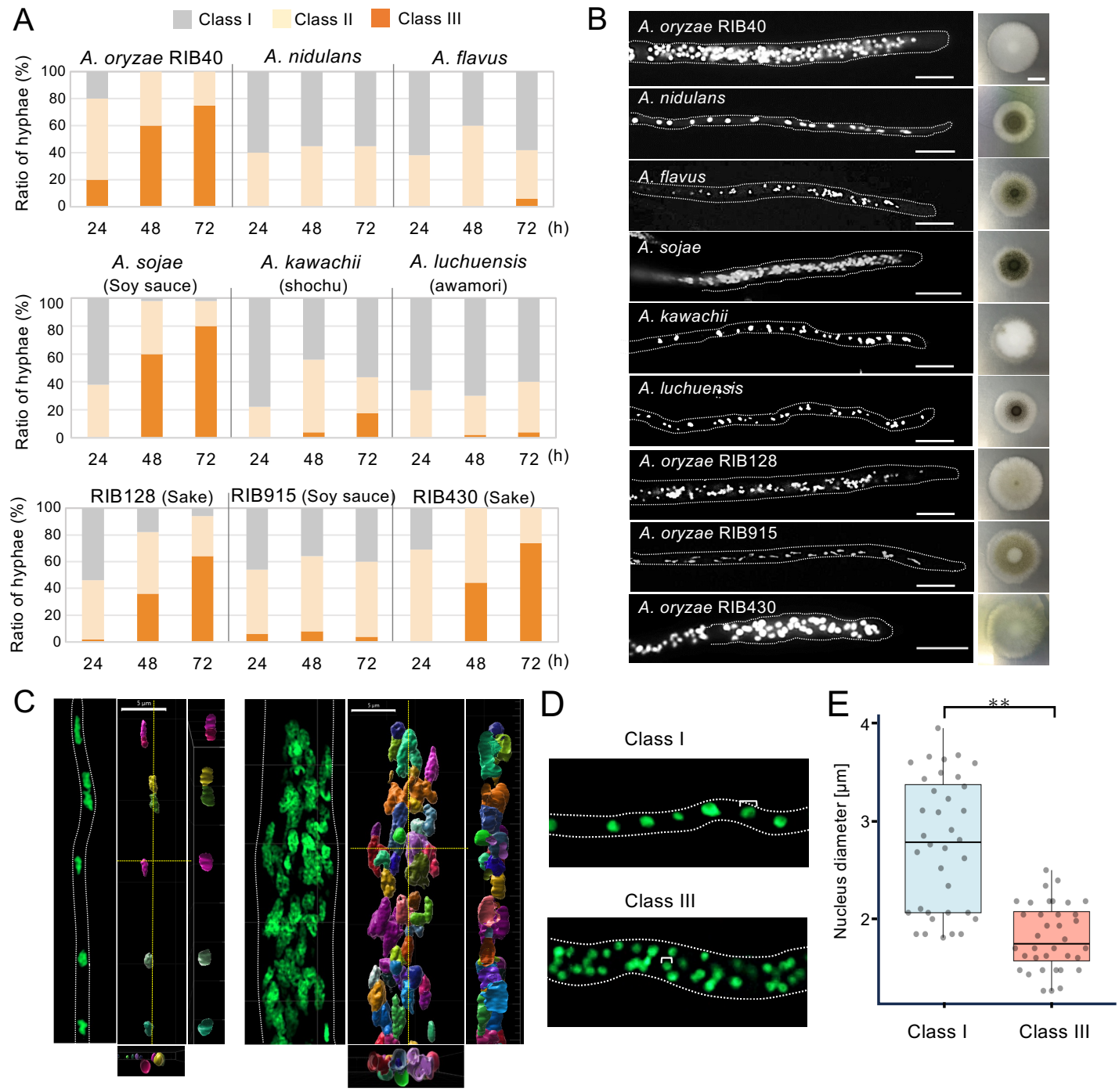
A
Class I
Class II
Class III
A. oryzae RIB40
A. nidulans
A. flavus
A. sojae (Soy sauce)
A. kawachii (shochu)
A. luchuensis (awamori)
RIB128 (Sake)
RIB915 (Soy sauce)
RIB430 (Sake)
Ratio of hyphae (%)
(h)
B
A. oryzae RIB40
A. nidulans
A. flavus
A. sojae
A. kawachii
A. luchuensis
A. oryzae RIB128
A. oryzae RIB915
A. oryzae RIB430
C
D
Class I
Class III
E
Nucleus diameter [μm]
Class I
Class III
F
Hyphal width [μm]
ns
RIB40
RIB128
RIB915
A. oryzae
A. sojae
A. nidulans
A. flavus
A. kawachii
A. luchuensis
G
RIB40
RIB128
RIB915
A. flavus
R² = 0.9392
Number of nuclei
Cell volume [×10³ μm³]

Fig. 2

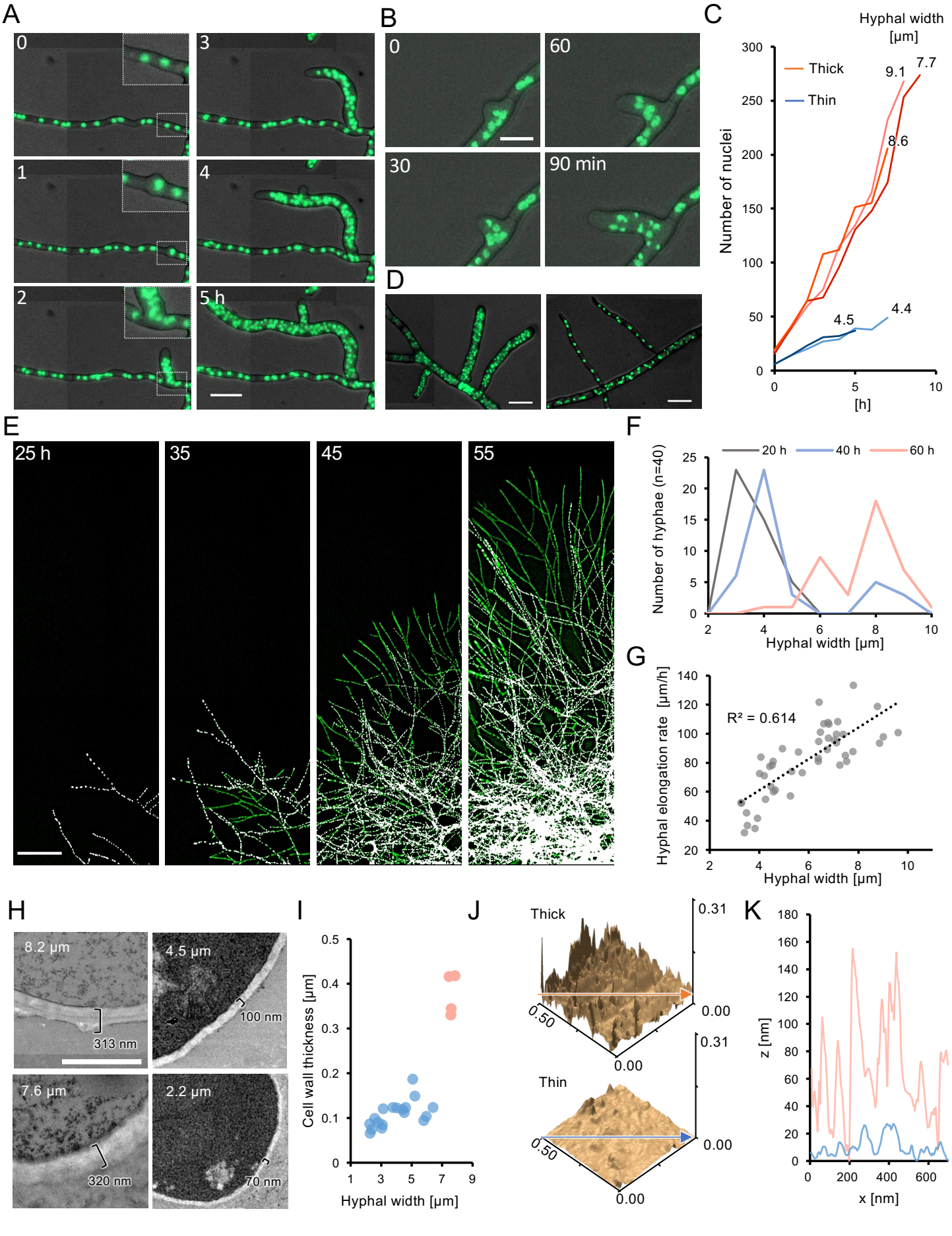
A
0
3
1
4
2
5 h
B
0
60
30
90 min
C
Hyphal width [µm]
Thick
Thin
9.1
7.7
8.6
4.5
4.4
Number of nuclei
[h]
D
E
25 h
35
45
55
F
20 h
40 h
60 h
Number of hyphae (n=40)
Hyphal width [µm]
G
R² = 0.614
Hyphal elongation rate [µm/h]
Hyphal width [µm]
H
8.2 µm
313 nm
4.5 µm
100 nm
7.6 µm
320 nm
2.2 µm
70 nm
I
Cell wall thickness [µm]
Hyphal width [µm]
J
Thick
Thin
0.31
0.00
0.50
K
z [nm]
x [nm]

Fig. 3

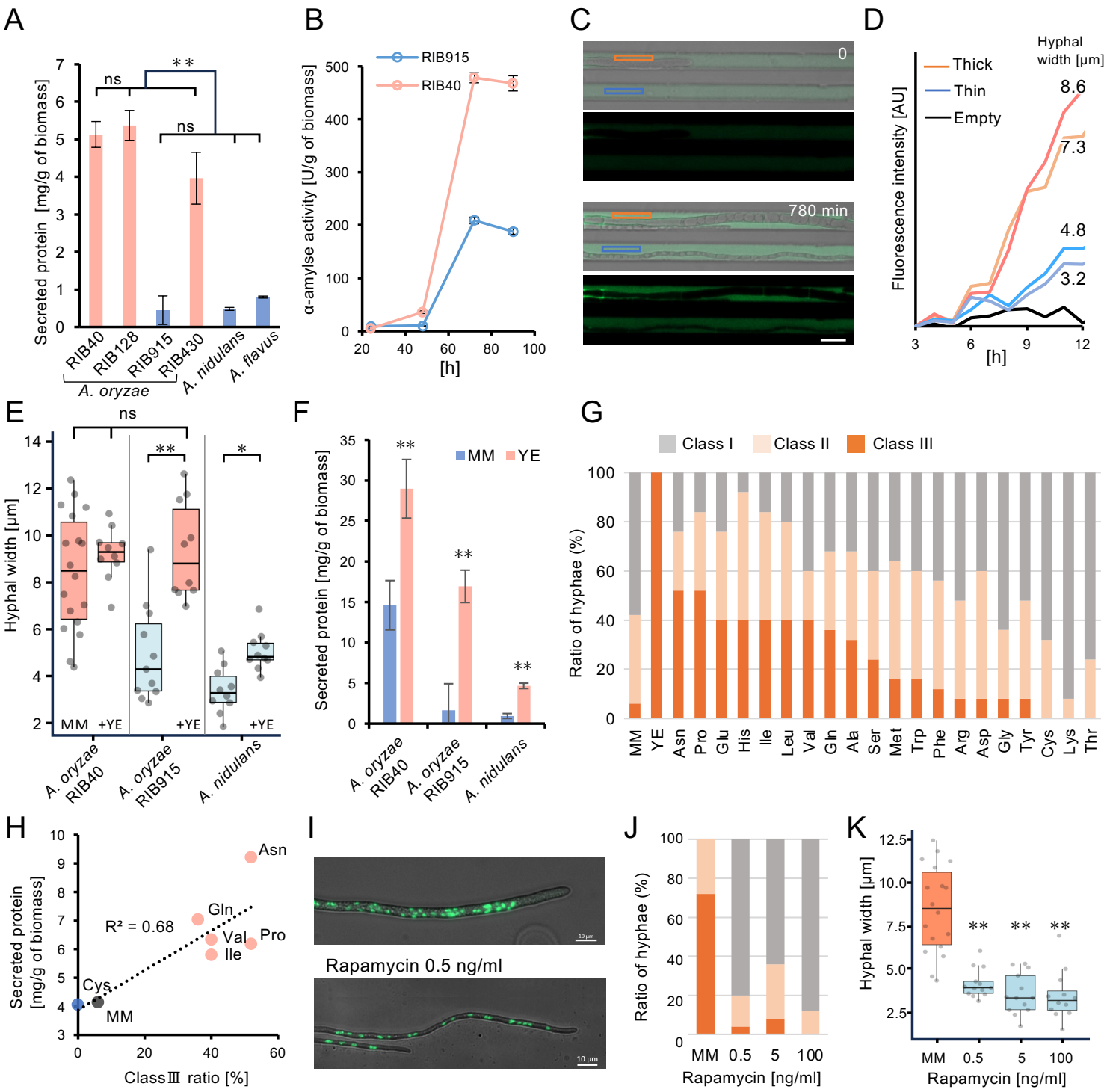
A
Secreted protein [mg/g of biomass]
ns
**
ns
RIB40
RIB128
RIB915
RIB430
A. nidulans
A. flavus
A. oryzae
B
α-amylse activity [U/g of biomass]
RIB915
RIB40
[h]
C
0
780 min
D
Hyphal width [μm]
Thick
Thin
Empty
8.6
7.3
4.8
3.2
Fluorescence intensity [AU]
[h]
E
Hyphal width [μm]
ns
**
*
MM
+YE
+YE
+YE
A. oryzae RIB40
A. oryzae RIB915
A. nidulans
F
Secreted protein [mg/g of biomass]
MM
YE
**
**
**
A. oryzae RIB40
A. oryzae RIB915
A. nidulans
G
Class I
Class II
Class III
Ratio of hyphae (%)
MM
YE
Asn
Pro
Glu
His
Ile
Leu
Val
Gln
Ala
Ser
Met
Trp
Phe
Arg
Asp
Gly
Tyr
Cys
Lys
Thr
H
Secreted protein [mg/g of biomass]
Asn
Gln
R² = 0.68
Val
Pro
Ile
Cys
MM
ClassⅢ ratio [%]
I
Rapamycin 0.5 ng/ml
10 μm
10 μm
J
Ratio of hyphae (%)
MM
0.5
5
100
Rapamycin [ng/ml]
K
Hyphal width [μm]
**
**
**
MM
0.5
5
100
Rapamycin [ng/ml]

Fig. 4

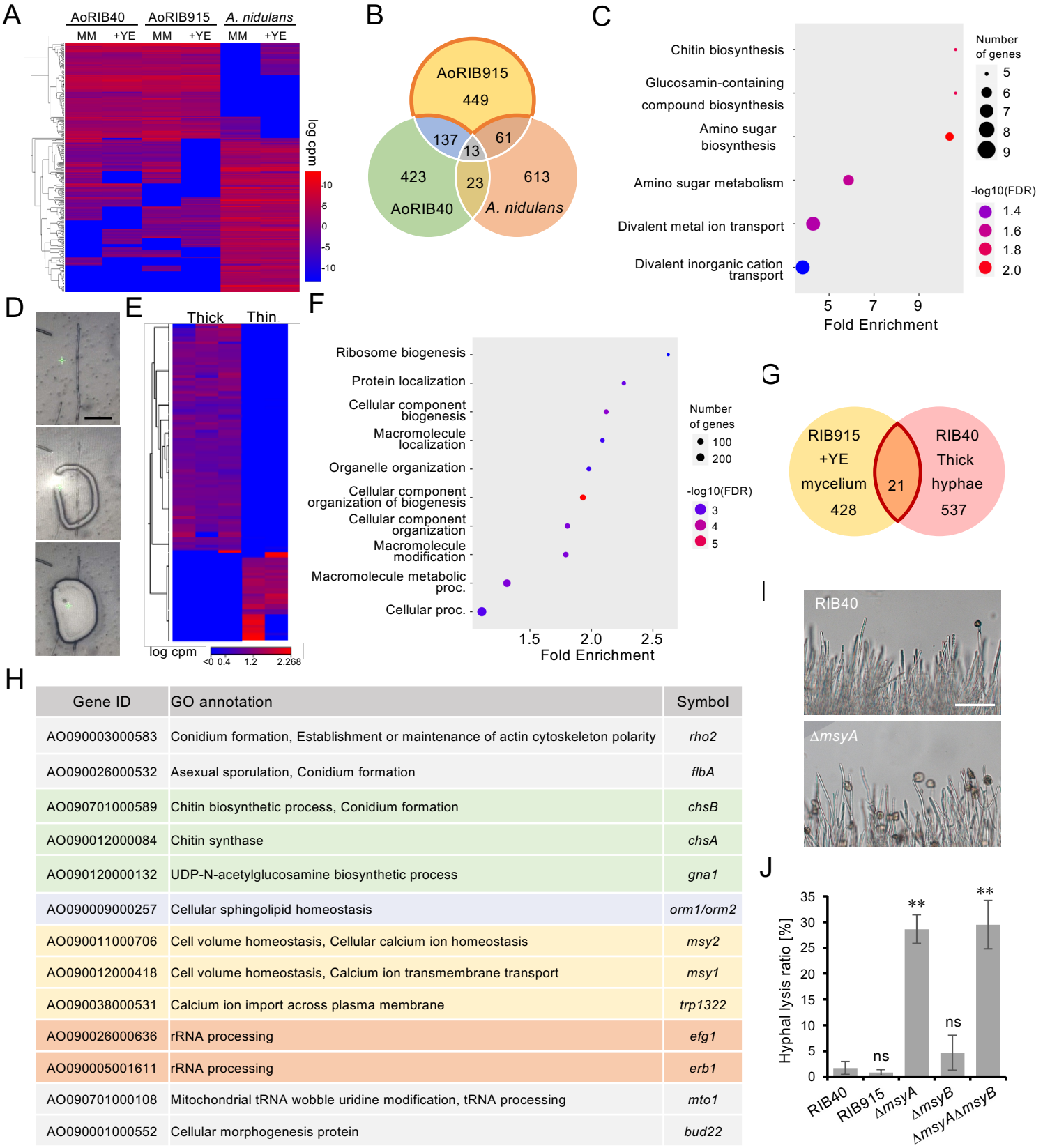

H

Gene ID	GO annotation	Symbol
AO090003000583	Conidium formation, Establishment or maintenance of actin cytoskeleton polarity	*rho2*
AO090026000532	Asexual sporulation, Conidium formation	*flbA*
AO090701000589	Chitin biosynthetic process, Conidium formation	*chsB*
AO090012000084	Chitin synthase	*chsA*
AO090120000132	UDP-N-acetylglucosamine biosynthetic process	*gna1*
AO090009000257	Cellular sphingolipid homeostasis	*orm1/orm2*
AO090011000706	Cell volume homeostasis, Cellular calcium ion homeostasis	*msy2*
AO090012000418	Cell volume homeostasis, Calcium ion transmembrane transport	*msy1*
AO090038000531	Calcium ion import across plasma membrane	*trp1322*
AO090026000636	rRNA processing	*efg1*
AO090005001611	rRNA processing	*erb1*
AO090701000108	Mitochondrial tRNA wobble uridine modification, tRNA processing	*mto1*
AO090001000552	Cellular morphogenesis protein	*bud22*

Fig. 5

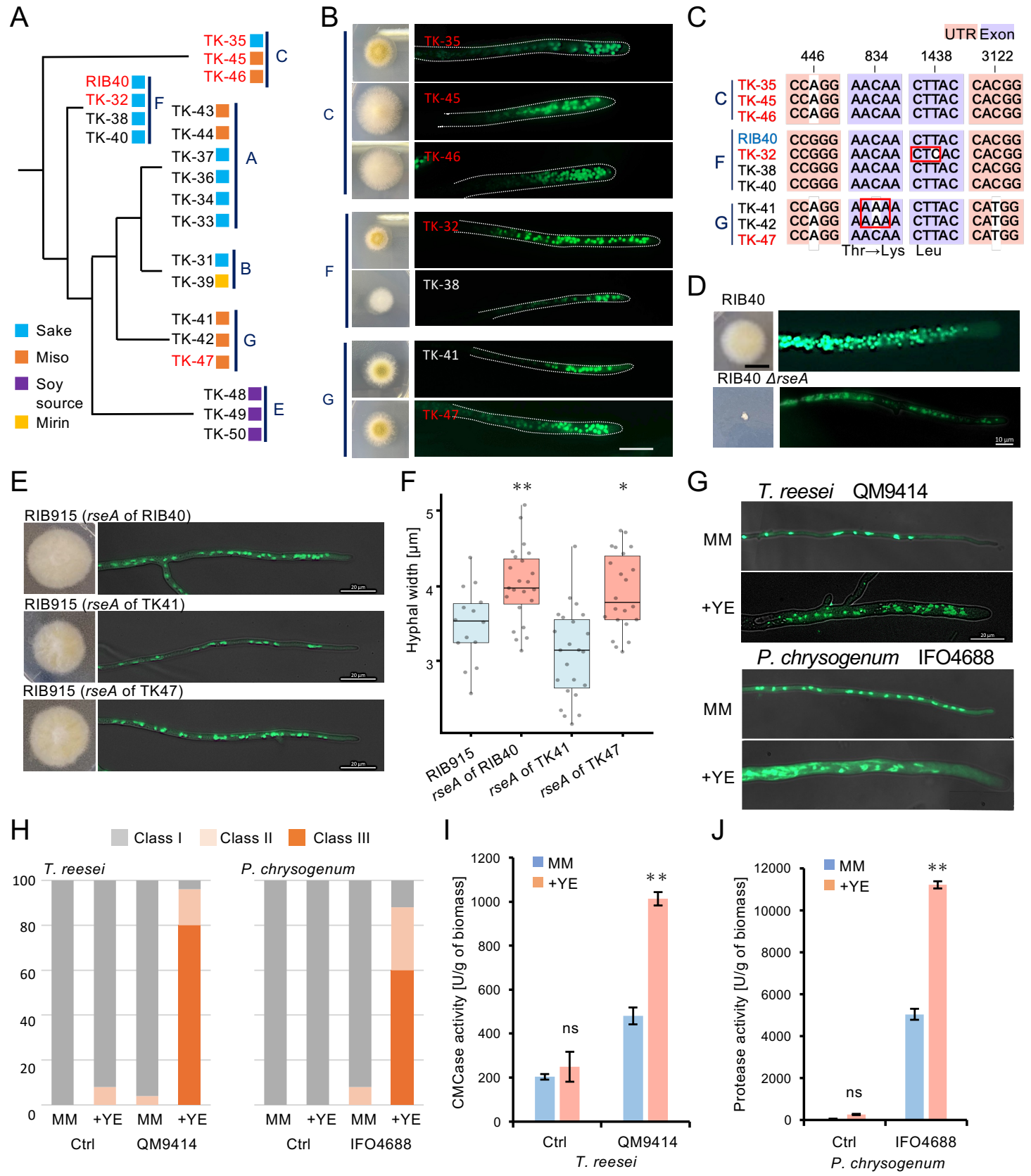
A
TK-35
TK-45
TK-46
C
RIB40
TK-32
TK-38
TK-40
F
TK-43
TK-44
TK-37
TK-36
TK-34
TK-33
A
TK-31
TK-39
B
TK-41
TK-42
TK-47
G
TK-48
TK-49
TK-50
E
Sake
Miso
Soy source
Mirin
B
C
F
G
TK-35
TK-45
TK-46
TK-32
TK-38
TK-41
TK-47
C
UTR Exon
446 834 1438 3122
C TK-35 CCAGG AACAA CTTAC CACGG
TK-45 CCAGG AACAA CTTAC CACGG
TK-46 CCAGG AACAA CTTAC CACGG
F RIB40 CCGGG AACAA CTTAC CACGG
TK-32 CCGGG AACAA CTCAC CACGG
TK-38 CCGGG AACAA CTTAC CACGG
TK-40 CCGGG AACAA CTTAC CACGG
G TK-41 CCAGG AAAAA CTTAC CATGG
TK-42 CCAGG AAAAA CTTAC CATGG
TK-47 CCAGG AACAA CTTAC CATGG
Thr→Lys Leu
D
RIB40
RIB40 ΔrseA
10 μm
E
RIB915 (rseA of RIB40)
RIB915 (rseA of TK41)
RIB915 (rseA of TK47)
20 μm
F
Hyphal width [μm]
5
4
3
**
*
RIB915
rseA of RIB40
rseA of TK41
rseA of TK47
G
T. reesei QM9414
MM
+YE
P. chrysogenum IFO4688
MM
+YE
20 μm
H
Class I
Class II
Class III
T. reesei
P. chrysogenum
100
80
60
40
20
0
MM +YE MM +YE
Ctrl QM9414
MM +YE MM +YE
Ctrl IFO4688
I
MM
+YE
CMCase activity [U/g of biomass]
1200
1000
800
600
400
200
0
ns
**
Ctrl
QM9414
T. reesei
J
MM
+YE
Protease activity [U/g of biomass]
12000
10000
8000
6000
4000
2000
0
ns
**
Ctrl
IFO4688
P. chrysogenum